Fast and artifact-free excitation multiplexing using synchronized image scanning

Ezra Bruggeman[1,2,‡], Robin Van den Eynde[1,‡], Baptiste Amouroux[1,a], Tom Venneman[3], Pieter Vanden Berghe[3], Marcel Müller[1], Wim Vandenberg[1,*], Peter Dedecker[1,*]

[1] Department of Chemistry, KU Leuven, 3001 Leuven, Belgium
[2] Yusuf Hamied Department of Chemistry, University of Cambridge, Cambridge CB2 1 EW, UK
[3] Department of Chronic Diseases Metabolism and Ageing, KU Leuven, 3001 Leuven, Belgium
[‡] Shared first author

[a] Present address: INSERM UMR 1148,
Université Sorbonne Paris Nord, Université Paris Cité, F- 93017, Bobigny, France

wim.vandenberg@kuleuven.be, peter.dedecker@kuleuven.be

Abstract

Multicolor fluorescence microscopy is an essential tool to visualize structures and dynamics in the life and materials sciences. However, the near-simultaneous acquisition of labels differing in excitation spectrum is difficult and renders such measurements prone to artifacts. We present a simple strategy to provide quasi-simultaneous fluorescence imaging with multiple excitation wavelengths, by using an optical element to displace the sample image on the sensor at a rate that is much faster than the image acquisition rate and synchronizing this with the illumination. The emission elicited by the different wavelengths can then be encoded into the point-spread function of the imaging or visualized as multiple distinct images. In doing so, our approach can eliminate or mitigate artifacts caused by temporal aliasing in conventional sequential imaging. We demonstrate the use of our system to uncover hidden emissive states in single quantum dots and for the imaging of Ca^{2+} signalling in neurons.

Key words: Fluorescence microscopy, multicolor imaging, point-spread function engineering, single-molecule spectroscopy, biosensor imaging

Multicolor fluorescence microscopy is a workhorse technique in the life and materials sciences because it allows multiple processes to be visualized and monitored within the same sample. To prevent distortions and artifacts, the different color channels must be acquired in a timespan that is short compared to the dynamics of the sample. In many cases sequential ('one by one') acquisitions of the different channels is the gold standard, though this can readily lead to temporal aliasing artifacts and distortions when the sample dynamics occur on faster time scales.

Such artifacts can be avoided by acquiring the different color channels simultaneously. This is easy to do when the channels differ in emission spectrum and can therefore be straightforwardly split using dichroic mirrors and optical filters. In sufficiently sparse (containing a low number of emitters) samples, the information on the emission color may also be obtained in other ways, such as the direct analysis of the shape of the point-spread function (PSF)[1], possibly enhanced by PSF engineering[2–5], or the introduction of a dispersive optical element such as a prism[6,7] or diffraction grating[8–10]. Overall, the simultaneous acquisitions of multiple emission bands works well because the full required information (the wavelength of the emission light) is contained within the emitted photons themselves.

Far fewer solutions exist when the fluorescence is to be distinguished based on differences in the excitation spectra of the emitters. This need is encountered in a variety of situations, such as the use of excitation-ratiometric biosensors[11,12], (single-molecule) FRET[13,14], single-molecule localization microscopy[15], or when

studying the spectroscopy of complex photochemical systems such as quantum dots[16]. The (near-) simultaneous multiplexing based on excitation wavelength is a much more difficult challenge because an emission photon does not 'know' the excitation wavelength that caused it to be emitted. As a result, sequential acquisitions remain the gold standard for excitation multiplexing, and temporal aliasing issues can readily arise except in select cases where the information content is limited. A number of alternative strategies have been explored, such as the encoding the excitation wavelength in the temporal modulation of the light sources[15,17,18] or stroboscopic illumination[19], though these all induce temporal delays and reduce the measurement bandwidth if the sample is to be monitored continuously.

In this work, we develop near-simultaneous excitation multiplexing by synchronizing the illumination with rapid displacements of the sample image on a camera sensor. We can take advantage of fast and inexpensive optical elements such as resonant scanners or micro-mirror devices that easily provide scanning frequenties of tens of kHz, as well as the microsecond or faster modulation allowed by even inexpensive light sources. This concept shares similarity with recently-published work[20], though it enables the encoding of this information into the point-spread function (PSF) of the imaging, thus preserving the full field-of-view of the measurement in sufficiently sparse samples. We explore some of the possibilities enabled by this device by imaging fast dynamic processes occurring in single quantum dots as well as a biosensor reporting calcium dynamics in hippocampal neurons.

Optical design

The overall design of our system is shown in figure 1a. The key feature of this design is the introduction of a resonant scanner into the emission beampath, which induces fast and periodic image displacements on the camera sensor. Such scanners are broadband mirrors that continuously and reliably oscillate at a fixed frequency up to tens of kHz depending on their construction, and that are furthermore available at modest expense. To complete the optical pipeline, we also introduced two additional lenses: a lens that collimates the light focused by the microscope tube lens, and a second lens that focuses the scanned light onto the camera.

Activating the resonant scanner results in the formation of a 'smeared-out' image under continuous illumination (figure 1b), caused by the fluorescence image being rapidly shifted over the detector by the motion of the resonant scanner. This 'smearing' effect occurs because the scanning frequency is much faster than the camera acquisition rate, which is usually in the tens of milliseconds or longer regime. We reasoned that this effect could be avoided by synchronizing the illumination with the motion of the scanner, illuminating with one illumination wavelength when the mirror is close to one of its turnaround points, and with a second illumination wavelength when the mirror is close to the other turnaround point (figure 1c). The net result is that a single emitter appears as two different spots in the image, where each spots provides the emission excited by one of the wavelengths. The distance between the spots is governed by the scan amplitude (figure 1d) and their shape is determined by the duty cycle of the illumination (figure 1e and supplementary note S2), defined here as the percentage of the time that at least one of the light sources is active. If the illumination duration can be made sufficiently short by using high-intensity light sources, more excitation wavelengths can furthermore be introduced at additional points of the scanning cycle. The relative brightness of the spots is determined by the relative light intensities and the efficiency with which the emitter can be excited by the different wavelengths. Our device thus provides an estimate of the excitation efficiencies for every emitter within the sample.

The crucial advantage of this device is the fast operation enabled by the resonant scanner, encoding very fast spectral information while retaining the full-field of view. Using a scanner operating at 16 kHz, for example, the time to switch between excitation wavelengths is only 31 µs, which is orders of magnitude faster than conventional sequential acquisitions, and also independent of the rate at which images are acquired since the signals are simply integrated by the camera. While the device does not increase the overall image acquisition speed, and hence in principle does not allow more frequency content to be acquired, it does strongly mitigate the possibility of aliasing artifacts since both excitation wavelengths are probed very rapidly and over the full duration of the acquisition, as we show using simulated data in figure 1f. In this figure and what follows, we denote the emission excited by irradiating using a wavelength λ as 'emission$_\lambda$'. As this figure shows, fast dynamics in the excitation efficiencies of a sample readily lead to distortions in sequential imaging, which can be efficiently suppressed using our approach.

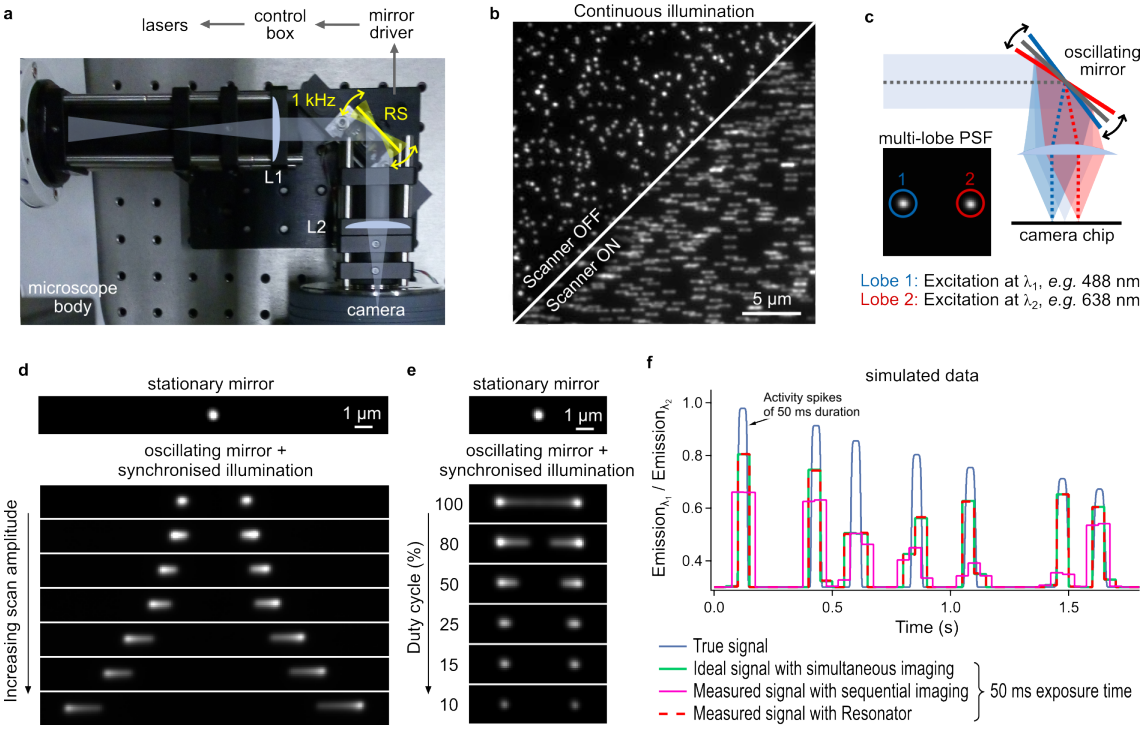

Figure 1: Concept. (a) Optical layout of the design including two relay lenses (L1 and L2) and the resonant scanner (RS) that displaces the image on the camera at 1 kHz. **(b)** Image of fluorescent beads (0.1 µm Tetraspeck beads) with and without oscillating motion of the scanner and 100% illumination duty cycle (continuous illumination). **(c)** Schematic illustration showing the synchronization of the illumination with the scanner motion. **(d)** Image of a single fluorescent bead showing the response of the system for different scanning amplitudes. **(e)** Image of a single fluorescent bead showing the response of the system for different duty cycles of the illumination. **(f)** Simulated data showing the (near-) elimination of aliasing artifacts using the Resonator. The blue line shows simulated ground-truth data resembling the fast response of an excitation-ratiometric biosensor. The green trace shows the ideal but experimentally infeasible responses for true simultaneous measurements using a finite camera exposure time. The magenta and red traces show the expected responses for sequential imaging and the use of our Resonator with a resonant scanner running at 1 kHz. Higher frequencies of the resonant scanning render the signal indistinguishable from the true simultaneous (green) trace.

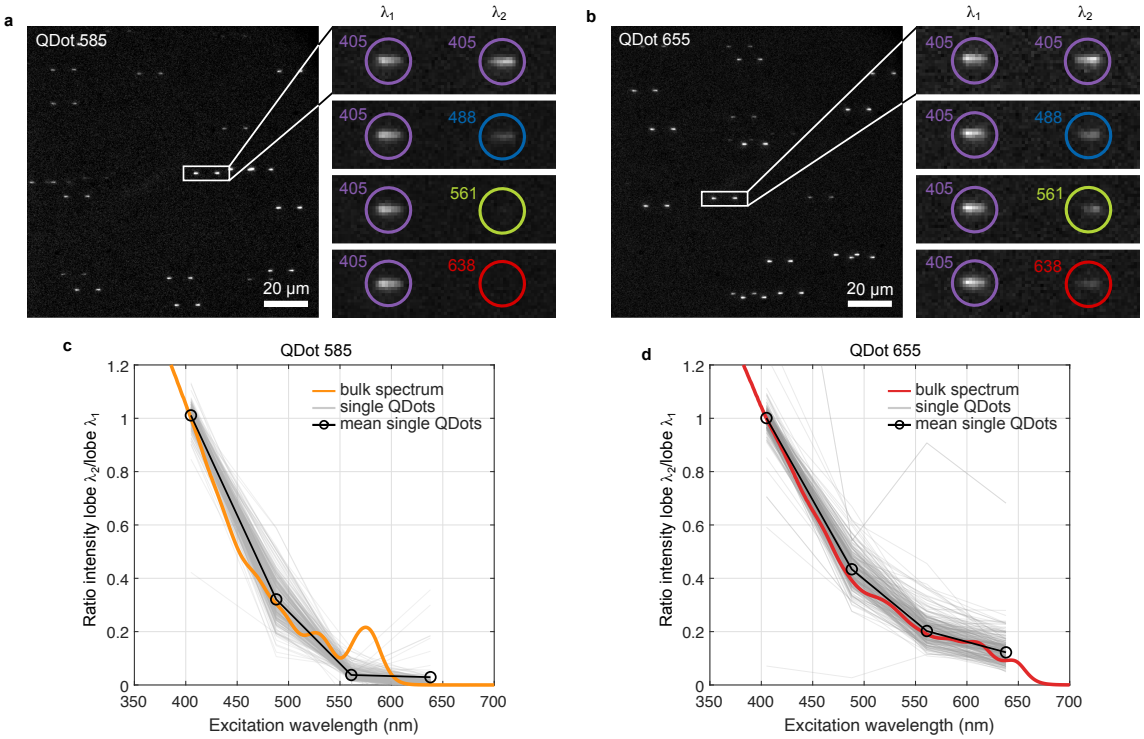

Figure 2: Probing the excitation spectra of single quantum dots. (a) Example image obtained on QDot585 emitters, where the inset shows different combinations of the illumination wavelengths. **(b)** Same as panel (a) but for QDot655. **(c)** Fluorescence intensities observed at the different excitation wavelengths normalized to the intensity observed with 405 nm excitation (n = 293 quantum dots from 14 fields of view). The colored line shows part of the excitation spectrum provided by the quantum dot supplier. **(d)** Same as panel (c) but for QDot655 (n = 231 quantum dots from 14 fields of view).

Alias-free imaging of single quantum dots

We explored the usefulness of our device via the imaging of single CdSe/ZnS core-shell type quantum dots. This type of emitters has attracted great interest on account of their high brightness, high photostability, and narrow emission spectra[16]. However, they are also well-known for their complex excited-state dynamics, including pervasive fluorescence dynamics that occur over a broad range of timescales[21]. We imaged immobilized quantum dots with emission spectra centered at 655 nm (QDot655) and 585 nm (QDot585) using our device (figure 2a-b), ensuring that the illumination intensities of the lasers were identical such that the ratio of the observed emission spots should reflect the excitation efficiencies of the quantum dots at the used excitation wavelengths. The resulting per-lobe intensities aligned with the bulk excitation spectra (figure 2a-b), showing that our Resonator indeed encodes the excitation efficiencies of the fluorophores.

We next turned our attention to monitoring the fluctuations in the emission of individual quantum dots. We again immobilized QDot655 emitters on a cover glass and measured their emission over 5000 fluorescence images with a 50 ms exposure time (total duration approximately four minutes), using excitation light at 488 and 638 nm. A single image from such a dataset is shown in figure 3a.

Figure 3b shows a kymograph from an intensity timetrace measured on a single quantum dot, showing the fluorescence intensities observed for each of the excitation wavelengths. Figure 3c shows the same data in a conventional graph. As expected, the traces show pronounced intermittencies on fast timescales. To compare these 'Resonator'-based acquisitions with conventional sequential acquisitions, we generated a derived dataset that mirrors conventional sequential acquisitions. We did this by including the fluorescence observed from only one of the excitation wavelengths in each image, alternating between the excitation wavelengths in consecutive frames. In other words, we consider only the intensity of the first PSF lobe in image i and only the intensity of the second lobe in image $i+1$, repeating this procedure for the full duration of the acquisition. The resulting intensity timetrace is shown in figure 3d. Comparison of the Resonator-based and sequential timetraces show that the sequential acquisitions lead to clear aliasing artifacts, evident in mismatches between the 488 nm and 638 nm excitation intensity traces. Selected instances of this are highlighted using the green markers in figure 3d.

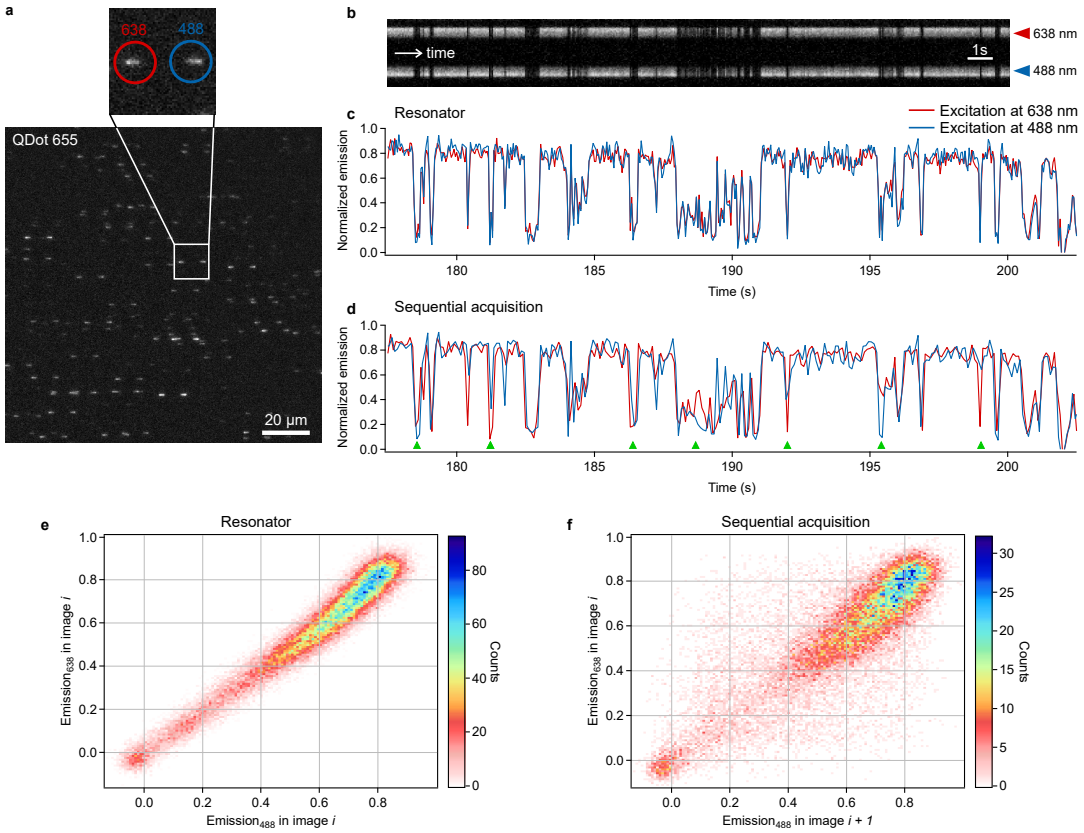

Figure 3: The Resonator suppresses aliasing artifacts in blinking quantum dots. (a) Example fluorescence image showing single QDot655 emitters. **(b)** Kymograph excerpt of the quantum dot highlighted with the inset in panel (a). **(c)** Intensity time traces of the quantum dot from panel (a). **(d)** Time traces calculated from those in panel (c) to approximate the effects of classical sequential acquisitions without the Resonator. The green triangles highlight events where artifacts due to temporal aliasing can be observed, though more artifacts can be seen. **(e)** 2D histogram of the fluorescence intensities observed in each image for the Resonator data in panel (c). **(f)** 2D histogram of the fluorescence intensities observed in each image for the calculated sequential acquisition data in panel (d).

The temporal aliasing seen in sequential acquisitions can suggest the presence of molecular states that do not in fact exist. To illustrate this, we plotted the fluorescence intensity observed upon 638 nm excitation against that observed upon 488 nm excitation, using both the native Resonator data and the sequential-like dataset described above (figure 3e and f). The sequential data shows a main fluorescent population but also shows broadly scattered intensities suggesting the presence of molecular states with shifted excitation spectra that absorb one of the excitation wavelengths more strongly. However, the Resonator data shows that the intensities of the two lobes are highly correlated, indicating that the data can be adequately explained as blinking involving a single fluorescent state with a constant excitation spectrum. These observations readily demonstrate the value of our device for the distortion-free measurement of fast processes occurring in systems such as optically active nanoparticles.

Simultaneous excitation and emission spectroscopy of quantum dots

We next sought to incorporate both excitation and emission information into the measurement. To do so, we placed a 630 nm long pass dichroic mirror in close proximity to the resonant scanning mirror, as shown in figure 4a. This configuration creates a PSF with 3 spots, where the relative intensities of the spots depend on both the emission and excitation spectra of the emitter: fluorescence photons with emission above 630 nm are transmitted by the dichroic mirror, creating two emission spots as previously described, while photons with a wavelength below 630 nm are reflected by the dichroic mirror and create a third emission spot regardless of the excitation wavelength that gave rise to this emission. Both emission bands are further separated by the presence of optical filters that block the 638 nm laser illumination.

Figure 4b shows an example fluorescence image and expansions acquired on QDot665 emitters, showing a high spectral diversity in the emission of the individual quantum dots. This diversity was evident also in the individual quantum dot timetraces, an example kymograph of which is shown in figure 4c. In addition to undergoing transitions in excitation and emission spectra, the quantum dots were also observed to undergo a blueshift upon irradiation, which has been widely described as 'spectral blueing'. This effect has been attributed to a decrease in quantum dot size due to photo-oxidation[22–24] with a rate that depends on the excitation wavelength[25].

Figure 4d analyzes the spectral diversity in more detail by showing the relative intensities of the 488 and 648 nm-excited fluorescence emitted above 630 nm for this particular quantum dot. Most of the data points appear to lie on a single line, suggesting the presence of dynamics involving a fluorescent state with constant excitation efficiences for both excitation wavelengths. Figure 4e, in contrast, approximates what would be observed using a classical sequential acquisition, revealing a more scattered distribution of the intensities that is much less straightforward to interpret. The intensity of the third PSF lobe provides information on the emission spectrum of the quantum dot, confirming a gradual blueing of the emission towards shorter wavelengths (figure 4f).

Closer inspection of figure 4d shows the presence of several data points that do not align with the overall trend, indicated with green markers on the graph. These points highlight the presence of a third state characterized by a higher efficiency for 488 nm excitation compared to 648 nm excitation. While these points can also be observed in the sequential data, they are obscured by the scattering induced by the temporal aliasing (figure 4e). Figure 4f additionally reveals that this third state has an emission spectrum in between the two detected wavelength bands. However, this data does not easily reveal whether additional points may also have arisen from this state but are intermingled with observations made on other states. To enhance the discriminatory power of this analysis, we visualized information from all three PSF lobes at once by graphing the fraction of the emission that the Resonator lobes contribute to the total detected quantum dot fluorescence in each image (figure 4g). In this figure, three different states can be clearly discerned, with state 1 the initial state, state 2 the state obtained upon emission blueing, and state 3 the intermediate state that is transiently formed in the measurement. This finding highlights the additional information enabled by our device.

Ratiometric Ca^{2+} sensing in firing neurons

The previous experiments used small scanning angles of the resonant mirror in order to encode the excitation information into the PSF, which allowed the full field-of-view of the single camera to be retained. Our device can also be used in a more classical image splitting arrangement by increasing the amplitude of the resonant scanner movement combined with the introduction of a field stop (figure 5a). The responses to the different

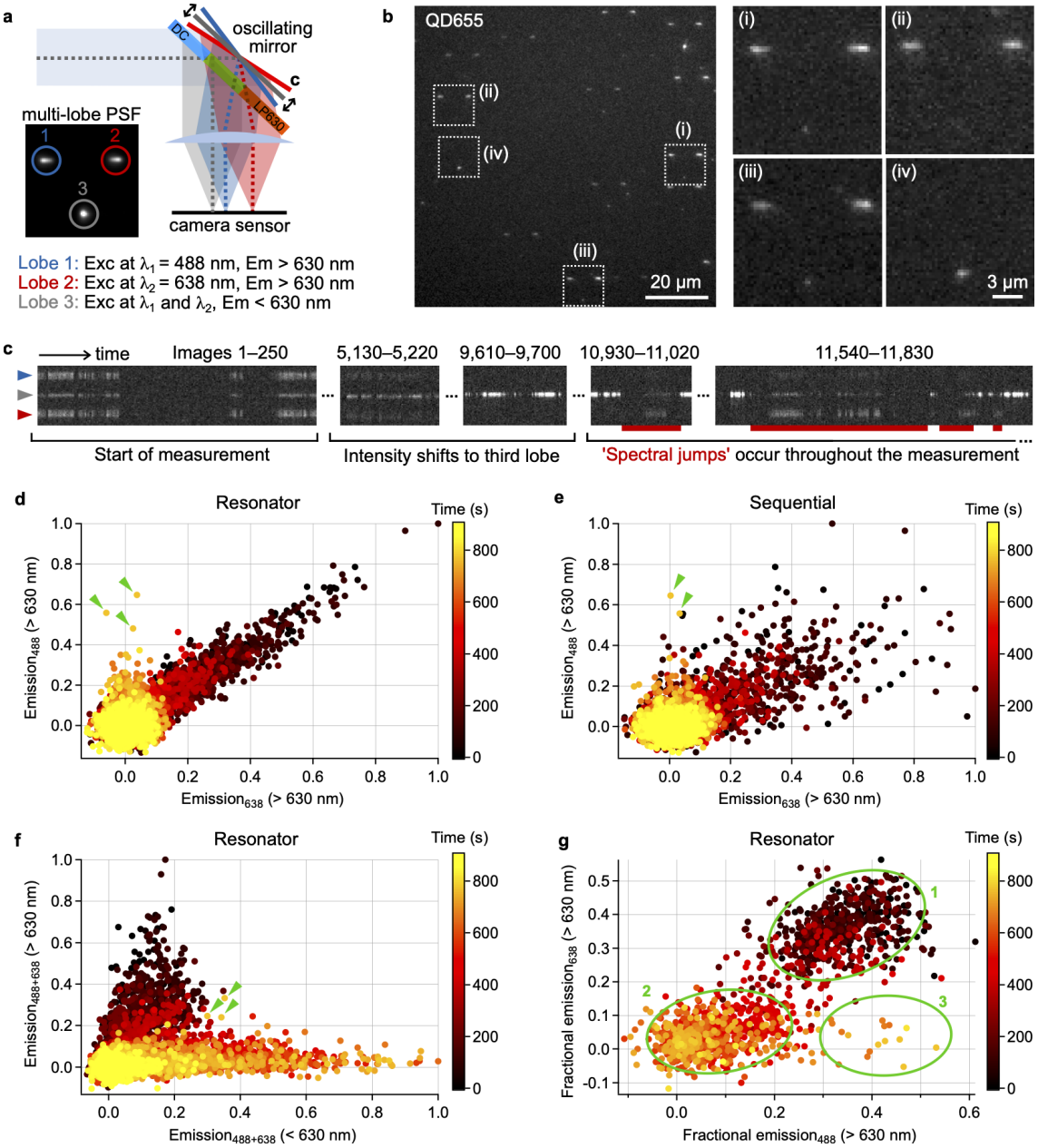

Figure 4: Combined single quantum dot excitation and emission spectroscopy. (a) Schematic illustration of the three-lobe optical setup. **(b)** Example image of quantum dots (QD655) on a cover glass, with 4 insets showing varying intensity distributions indicating spectral differences. **(c)** Kymogram showing spectral dynamics in a single QDot655 emitter. A limited set of intervals of interest has been selected. **(d)** Temporally colour-coded scatter plot of the intensities observed in the excitation lobes emitting above 630 nm. The green markers in this and following panels are discussed in the main text. Small negative values in these and the following panels arise from the use of background subtraction in the presence of measurement noise. **(e)** Calculated sequential acquisition data approximating what would be observed for the data in panel (d) without the Resonator. **(f)** Temporally color-coded scatter plot distribution of the emission intensities above and below 630 nm. **(g)** Temporally color-coded scatter plot of showing the fractional contribution of the indicated emission to the total emission (sum of the three lobe intensities) observed in each image. To enhance the visual clarity, only images in which the total emissionwas over a threshold were included in this visualization, as is discussed in more detail in the materials and methods section.

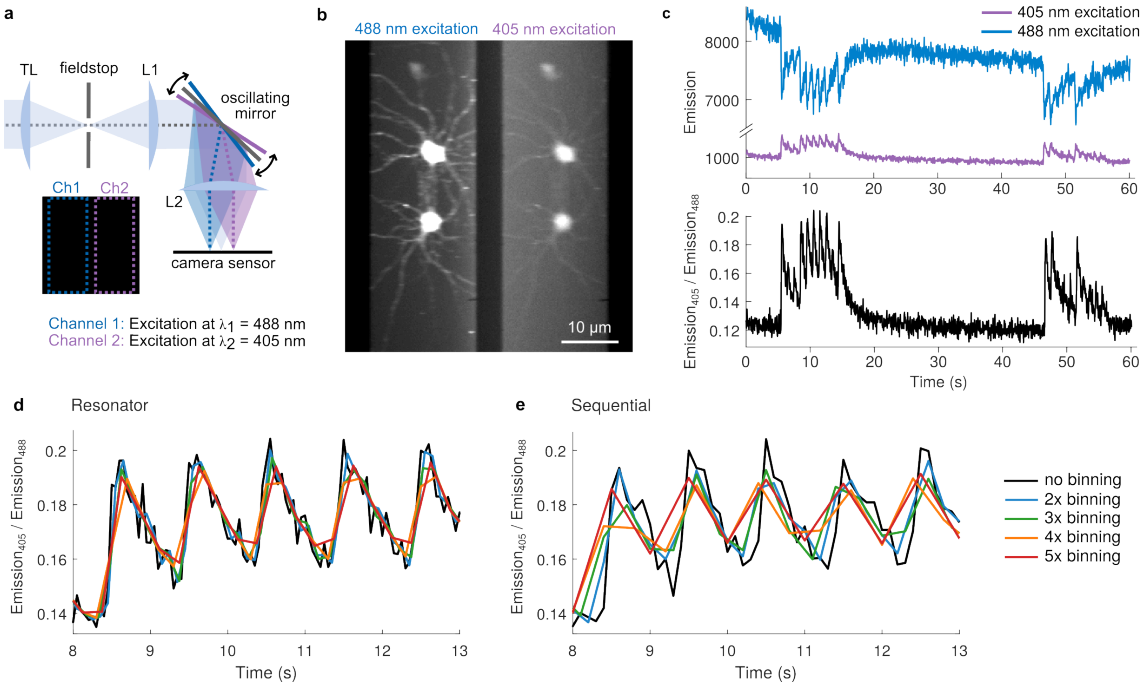

Figure 5: Ratiometric calcium imaging in firing hippocampal neurons. (a) Schematic illustration of the optical layout. **(b)** Average image calculated from all 1560 fluorescence images acquired on two neurons, showing the two excitation channels. The color lookup table is different for the 405 and 488 nm image so that both channels are similarly observable. The color lookup table in this image was clipped due to the large differences in brightness between the cell body and dendrite structures. A log-color version of this image can be found as supplementary figure S1. **(c)** Integrated intensities observed for the upper cell from panel (b) as the ratio of the intensities. **(d)** Calculation of the excitation ratios for different temporal binning values. **(e)** Same as panel (e) but for calculated sequential acquisitions.

excitation wavelengths then appear as distinct regions on the camera sensor, essentially mirroring the use of a conventional image splitter for emission multiplexing, though we here deliver excitation multiplexing. One area where such a system finds obvious use is in the imaging of biosensors, fluorophores for which the emission is conditional on a well-defined aspect of their environment[26]. Within the large biosensor family, ratiometric biosensors encode this information as a change in the ratio of two excitation and/or emission wavelength regions. We chose to focus on the ratiometric Ca^{2+} biosensor FuraRed[12],which encodes the local calcium concentration into the ratio of the fluorescence intensities excited at 405 nm and 488 nm. The fast dynamics of neuronal signaling have given rise to multiple strategies to deliver faster excitation-ratiometric measurements (e.g.[27]).

We applied the Resonator to the imaging of Ca^{2+} dynamics in firing mouse hippocampal neurons, where the different excitation channels are imaged onto distinct regions of the image sensor (figure 5b). The action potentials are clearly visible from the intensity traces observed at each excitation wavelength as well as the ratio between them (figure 5c). We again compared our Resonator-based acquisition with a derived dataset showing what would be observed using sequential acquisitions, additionally varying the temporal resolution by binning adjacent images together. The calcium responses in these measurements were slow enough that comparatively little temporal aliasing arose even in sequential measurements because no spontaneous high-frequency firing is present in sparse cultures at room temperature. However, in more complex neuronal networks where neuronal firing frequencies can rise to several tens up to 100 Hz, in which case sequential imaging may well cause aliasing artifacts. Comparison of the Resonator-based and sequential measurements for binned data (figure 5d and e) clearly demonstrates that our device can indeed eliminate aliasing artifacts also under these conditions, showing that this strategy can also be applied to samples that are too dense to support PSF-encoding of the information or where such encoding is undesirable.

In conclusion, we have presented a strategy for near-simultaneous excitation multiplexing based on synchronizing the excitation light with fast displacements of the sample image on a camera sensor, in a format that can be combined both with image splitting and as a form of PSF engineering. We achieve this by introducing a rapidly oscillating mirror into the emission beam path, such that each fluorophore can be observed as two distinct emission spots corresponding to each of the excitation wavelengths. and in a way that al-

lows the scanning amplitude to be easily changed. Small amplitudes enable the use of the device for PSF engineering, while larger amplitudes and the introduction of a field stop allows more conventional image splitter-like operation. Further excitation wavelengths could be introduced by synchronizing their illumination with different ranges of the scanner motion. The resulting information can be used to provide (nearly) aliasing-free multicolor imaging based on difference in excitation spectra.

This crucial advantage arises because common resonant scanners readily provide scanning frequencies up to 16 kHz or faster, allowing the different excitation wavelengths to be probed within just a few tens of microseconds using comparatively inexpensive equipment. Compared to the per-image sequential acquisition usually used for excitation multiplexing, our method allows much faster sampling and eliminates (much of) the aliasing artifacts that otherwise lead to distortions in the measurement, as we demonstrated in this study using the imaging of quantum dots and hippocampal neurons. While this implementation has made use of a resonant scanner, our approach could also be combined with alternative fast scanning mirrors such as MEMS-based devices.

Our approach is complementary with the work detailed in Ref.[20], which permits a higher duty cycle of the illumination and hence higher sensitivity by introducing focusing lenses to avoid the PSF-broadening encountered here. A consequence of this is that the fluorescence emitted by the different excitation wavelengths must be focused onto different parts of the detector. As a result, the field-of-view must be reduced or alternatively retained via the introduction and alignment of multiple detectors, which is typically difficult to do for high-resolution imaging. However, this approach does bring the advantage that any possible background emission excited by the different illumination wavelengths does not impinge on the same image area. The strategy detailed here retains essentially the full field-of-view of just a single detector, yields lower sensitivity due to the reduced illumination time and higher sensitivity to background, but is far simpler to implement in practice.

This approach can also be combined with other functionalities to achieve additional information content. One example is the introduction of an additional, stationary, dichroic mirror that results in a three-lobe PSF, as we have demonstrated here. The approach could also be combined with conventional dichroic-mirror based image splitters, simultaneously delivering information on both the excitation and emission spectra, or with other PSF-engineering modalities such as the introduction of astigmatism or more complex phase manipulations to encode z-positions or emission spectra of the fluorophores.

In conclusion, we have developed a measurement strategy and matching optical device that deliver near-simultaneous excitation multiplexing in any situation where fast processes must be monitored by observing the fluorescence emitted in response to different excitation wavelengths. By providing (nearly) alias-free multiplexing based on excitation wavelength, our device readily expands the available strategies for multi-spectral fluorescence imaging and spectroscopy.

Acknowledgements

We thank Steven F. Lee (University of Cambridge) for discussions and support. R.V.D.E. thanks the Research Foundation-Flanders (FWO Vlaanderen) for a doctoral fellowship (1SB7219N) and the KU Leuven for a postdoctoral fellowship (PDMT2/23/043). M.M. was supported by Marie Skłodowska-Curie postdoctoral fellowship 752080 FASTR3DSIM. This work was supported by the European Research Council through grant 714688 NanoCellActivity, the Research Foundation-Flanders through grants G090819N, G086222N, and G010723N, and the KU Leuven via grant C14/22/088.

Author contributions

W.V., P.D., and M.M. designed research. P.D. supervised research. R.V.D.E., E.B., M.M., B.A., and W.V. constructed the optical device. E.B., R.V.D.E., T.V., and P.V.B. prepared samples. E.B., R.V.D.E., M.M, T.V., and P.V.B. performed experiments. E.B., W.V., and P.D. analyzed data. P.D. and E.B. wrote the manuscript with input from R.V.D.E. and W.V.

Supplementary information

Materials and methods section, photographs of the overall instrument, and a list of components used in the construction of the device.

Data availability

The experimental data and analysis code are available on Zenodo at `https://doi.org/10.5281/zenodo.10866431`.

References

1. Hershko, E., Weiss, L. E., Michaeli, T. & Shechtman, Y. Multicolor localization microscopy and point-spread-function engineering by deep learning. *Optics Express* **27,** 6158 (2019).
2. Shechtman, Y., Weiss, L. E., Backer, A. S., Lee, M. Y. & Moerner, W. E. Multicolour localization microscopy by point-spread-function engineering. *Nat. Photonics* **10,** 590–594 (2016).
3. Smith, C., Huisman, M., Siemons, M., Grünwald, D. & Stallinga, S. Simultaneous measurement of emission color and 3D position of single molecules. *Optics Express* **24,** 4996–5013 (2016).
4. Martens, K. J. A. *et al.* Enabling Spectrally Resolved Single-Molecule Localization Microscopy at High Emitter Densities. *Nano Letters* **22,** 8618–8625 (2022).
5. Van den Eynde, R. *et al.* Simultaneous multicolor fluorescence imaging using PSF splitting. *Nature Methods* (Accepted).
6. Zhang, Z., Kenny, S., Hauser, M., Li, W. & Xu, K. Ultrahigh-throughput single-molecule spectroscopy and spectrally resolved super-resolution microscopy. *Nature Methods* **12,** 935–938 (2015).
7. Jeffet, J. *et al.* Multimodal single-molecule microscopy with continuously controlled spectral resolution. *Biophysical Reports* **1,** 100013 (2021).
8. Broeken, J., Rieger, B. & Stallinga, S. Simultaneous measurement of position and color of single fluorescent emitters using diffractive optics. *Opt. Lett.* **39,** 3352–3355 (2014).
9. Mlodzianoski, M. J., Curthoys, N. M., Gunewardene, M. S., Carter, S. & Hess, S. T. Super-Resolution Imaging of Molecular Emission Spectra and Single Molecule Spectral Fluctuations. *PLOS ONE* **11** (2016).
10. Dong, B. *et al.* Super-resolution spectroscopic microscopy via photon localization. *Nature Communications* **7,** 12290 (2016).
11. Grynkiewicz, G., Poenie, M. & Tsien, R. Y. A new generation of Ca2+ indicators with greatly improved fluorescence properties. *The Journal of biological chemistry* **260,** 3440–50 (1985).
12. Lipp, P. & Niggli, E. Ratiometric confocal Ca2+-measurements with visible wavelength indicators in isolated cardiac myocytes. *Cell Calcium* **14,** 359–372 (1993).
13. Kapanidis, A. N. *et al.* Fluorescence-aided molecule sorting: analysis of structure and interactions by alternating-laser excitation of single molecules. *Proc. Natl. Acad. Sci. USA* **101,** 8936–8941 (2004).
14. Müller, B. K., Zaychikov, E., Bräuchle, C. & Lamb, D. C. Pulsed interleaved excitation. *Biophysical journal* **89,** 3508–3522 (2005).
15. Gómez-García, P. A., Garbacik, E. T., Otterstrom, J. J., Garcia-Parajo, M. F. & Lakadamyali, M. Excitation-multiplexed multicolor superresolution imaging with fm-STORM and fm-DNA-PAINT. *Proc. Natl. Acad. Sci. USA* **115,** 12991–12996 (2018).
16. Resch-Genger, U., Grabolle, M., Cavaliere-Jaricot, S., Nitschke, R. & Nann, T. Quantum dots versus organic dyes as fluorescent labels. *Nature Methods* **5,** 763–775 (2008).
17. Åslund, N. & Carlsson, K. Confocal scanning microfluorometry of dual-labelled specimens using two excitation wavelengths and lock-in detection technique. *Micron* **24,** 603–609 (1993).
18. Lewis, E. K. *et al.* Color-blind fluorescence detection for four-color DNA sequencing. *Proc. Natl. Acad. Sci. USA* **102,** 5346–5351 (2005).
19. Farooq, S. & Hohlbein, J. Camera-based single-molecule FRET detection with improved time resolution. *Physical Chemistry Chemical Physics* **17,** 27862–27872 (2015).
20. Wu, W. *et al.* Tetra-color superresolution microscopy based on excitation spectral demixing. *Light: Science & Applications* **12,** 9 (2023).

21. Efros, A. L. & Nesbitt, D. J. Origin and control of blinking in quantum dots. *Nature Nanotechnology* **11,** 661–671 (2016).
22. Cordero, S. R., Carson, P. J., Estabrook, R. A., Strouse, G. F. & Buratto, S. K. Photo-Activated Luminescence of CdSe Quantum Dot Monolayers. *The Journal of Physical Chemistry B* **104,** 12137–12142 (2000).
23. Van Sark, W. G. J. H. M., Frederix, P. L. T. M., Bol, A. A., Gerritsen, H. C. & Meijerink, A. Blueing, Bleaching, and Blinking of Single CdSe/ZnS Quantum Dots. *ChemPhysChem* **3,** 871–879 (2002).
24. Lee, S. F. & Osborne, M. A. Photodynamics of a Single Quantum Dot: Fluorescence Activation, Enhancement, Intermittency, and Decay. *Journal of the American Chemical Society* **129,** 8936–8937 (2007).
25. Ozasa, K., Nemoto, S., Maeda, M. & Hara, M. Excitation-wavelength-dependent photoluminescence evolution of CdSe/ZnS nanoparticles. *Journal of Applied Physics* **101,** 103503 (2007).
26. Van Thillo, T., Van Deuren, V. & Dedecker, P. Smart genetically-encoded biosensors for the chemical monitoring of living systems. *Chemical Communications* **59,** 520–534 (5 2023).
27. Vanden Berghe, P., Kenyon, J. L. & Smith, T. K. Mitochondrial Ca^{2+} uptake regulates the excitability of myenteric neurons. *The Journal of neuroscience : the official journal of the Society for Neuroscience* **22,** 6962–6971 (16 2002).

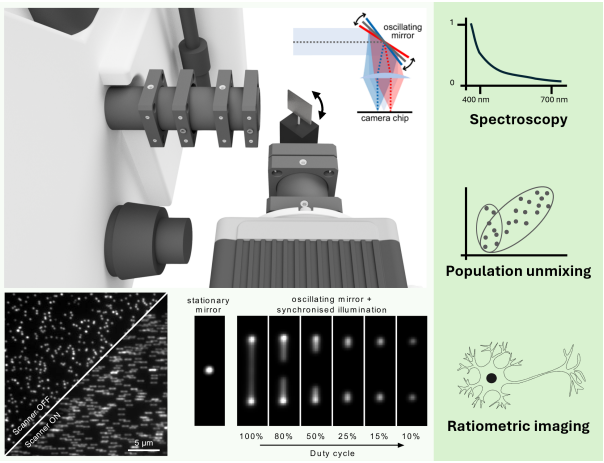

For Table of Contents Only